

Inertial range scaling in numerical turbulence with hyperviscosity

Nils Erland L. Haugen*

*Department of Physics, The Norwegian University of Science and Technology, Høy skoleringen 5, N-7034 Trondheim, Norway*Axel Brandenburg[†]*NORDITA, Blegdamsvej 17, DK-2100 Copenhagen Ø, Denmark*

(Received 13 February 2004; revised manuscript received 7 June 2004; published 26 August 2004)

Numerical turbulence with hyperviscosity is studied and compared with direct simulations using ordinary viscosity and data from wind tunnel experiments. It is shown that the inertial range scaling is similar in all three cases. Furthermore, the bottleneck effect is approximately equally broad (about one order of magnitude) in these cases and only its height is increased in the hyperviscous case—presumably as a consequence of the steeper descent of the spectrum in the hyperviscous subrange. The mean normalized dissipation rate is found to be in agreement with both wind tunnel experiments and direct simulations. The structure function exponents agree with the She-Leveque model. Decaying turbulence with hyperviscosity still gives the usual $\tau^{-1.25}$ decay law for the kinetic energy, and also the bottleneck effect is still present and about equally strong.

DOI: 10.1103/PhysRevE.70.026405

PACS number(s): 52.65.Kj, 47.11.+j, 47.27.Ak, 47.65.+a

I. INTRODUCTION

In recent years there has been growing awareness of the detailed structure of the kinetic energy spectrum of hydrodynamic turbulence. In addition to the basic Kolmogorov $k^{-5/3}$ spectrum with an exponential dissipation range there are strong indications of intermittency corrections (possibly throughout the entire inertial range) and there is also the so-called bottleneck effect [1,2], i.e., a shallower spectrum near the beginning of the dissipative subrange; see also Ref. [3]. These features can be seen both in high resolution simulations [4] and in measurements of wind tunnel turbulence [5].

Over the past few years it has become evident that in numerical turbulence the bottleneck effect is rather pronounced [4,6,7]. However, some of the simulations used hyperviscosity or other kinds of subgrid scale modeling. Hyperviscosity has frequently been used in turbulence studies in order to shorten the dissipative subrange [8–12]. However, hyperviscosity has also been suggested as a possible source of an artificially enhanced bottleneck effect [13,14]. Meanwhile, the apparent discrepancy in the strength of the bottleneck effect between simulations and experiments has been identified as being due to the difference in the diagnostics: in wind tunnel experiments one is only able to measure one-dimensional (longitudinal or transversal) energy spectra, while in simulations one generally considers shell integrated three-dimensional spectra. The two are related by a simple integral transformation [15–17]. It turns out that, while the bottleneck effect can be much weaker or even completely absent in the one-dimensional spectrum, it is generally much stronger in the three-dimensional spectrum [18].

In order to see the bottleneck effect in simulations, it is important to have sufficiently large resolution of around

1024^3 meshpoints. This raises the question of to what extent the bottleneck effect seen in simulations with hyperviscosity is an artifact or a real feature that becomes noticeable only above a certain resolution. It is thus possible that the reason for an exaggerated bottleneck effect in the hyperviscous simulation is related to the fact that hyperviscosity increases the effective resolution beyond the threshold above which the bottleneck effect can be seen.

In this paper we consider forced hydrodynamic turbulence using hyperviscosity proportional to ∇^6 (instead of the usual ∇^2 viscosity operator). We find that the bottleneck effect is enhanced in amplitude—but not in width, compared with direct simulations at the currently largest resolution of 4096^3 on the Earth Simulator [4]. One of the important results of these very high resolution simulations is that an inertial range begins to emerge that is clearly distinct from the bottleneck effect. Furthermore, the (negative) slope in the inertial range is steeper than the standard Kolmogorov power law exponent of $5/3$ by about 0.1, so it is approximately 1.77.

As in earlier papers [18], we consider weakly compressible turbulence using an isothermal equation of state. The root mean square Mach number is between 0.12 and 0.13; for this type of weakly compressible simulations, we find that the energies of solenoidal and potential components of the flow have a ratio $E_{\text{pot}}/E_{\text{sol}} \approx 10^{-4} - 10^{-2}$ for most scales; only towards the Nyquist frequency the ratio increases to about 0.1. Compressibility is therefore not expected to play an important role.

II. BASIC EQUATIONS

We solve the compressible Navier-Stokes equations

$$\frac{D\mathbf{u}}{Dt} = -\frac{1}{\rho} \nabla p + \mathbf{f} + \mathbf{F}_{\text{visc}}, \quad (1)$$

where $D/Dt = \partial/\partial t + \mathbf{u} \cdot \nabla$ is the advective derivative, p is pressure, ρ is the density, \mathbf{f} is an isotropic, random, nonheli-

*Electronic address: nils.haugen@phys.ntnu.no

[†]Electronic address: brandenb@nordita.dk

cal forcing function with power in a narrow band of wave numbers, and

$$\mathbf{F}_{\text{visc}} = \frac{1}{\rho} \nabla \cdot (2\rho\nu_n \mathbf{S}^{(n)}) \quad (2)$$

is the viscous force. Here,

$$\mathbf{S}^{(n)} = (-\nabla^2)^{n-1} \mathbf{S} \quad (3)$$

is a higher order traceless rate of strain tensor

$$\mathbf{S}_{ij} = \frac{1}{2}(u_{i,j} + u_{j,i}) - \frac{1}{3}\delta_{ij} \nabla \cdot \mathbf{u} \quad (4)$$

is the usual traceless rate of strain tensor, and commas denote partial differentiation. In the following we restrict ourselves to the case where $\mu_n \equiv \rho\nu_n = \text{const}$. Using the product rule, we can then rewrite Eq. (2) in the form

$$\mathbf{F}_{\text{visc}} = (-1)^{n-1} \frac{\mu_n}{\rho} (\nabla^{2n} \mathbf{u} + \frac{1}{3} \nabla^{2(n-1)} \nabla \nabla \cdot \mathbf{u}). \quad (5)$$

For $n=1$ we recover the normal diffusion operator for compressible flows. In the present paper we choose $n=3$, so Eq. (5) reduces to

$$\mathbf{F}_{\text{visc}} = \frac{\mu_3}{\rho} (\nabla^6 \mathbf{u} + \frac{1}{3} \nabla^4 \nabla \nabla \cdot \mathbf{u}). \quad (6)$$

In the incompressible case, which is usually considered, the second term in Eq. (6) vanishes. However, in the compressible case considered here this term is important to ensure momentum conservation. The local rate of kinetic energy dissipation per unit mass is

$$\epsilon = 2\mu_3 (\nabla^2 \mathbf{S})^2, \quad (7)$$

which is positive definite.

We consider an isothermal gas with constant sound speed c_s , so that the pressure is given by $p = c_s^2 \rho$ and $\rho^{-1} \nabla p = c_s^2 \nabla \ln \rho$. The density obeys the continuity equation

$$\frac{D \ln \rho}{Dt} = -\nabla \cdot \mathbf{u}. \quad (8)$$

For all our simulations we have used the PENCIL CODE [19], which is a grid based high order code (sixth order in space and third order in time) for solving the compressible hydrodynamic equations.

III. RESULTS

We have calculated a series of models with resolutions varying between 64^3 and 512^3 meshpoints using a third order hyperviscosity ($n=3$). When changing the resolution, we keep the grid Reynolds number, here defined as

$$\text{Re}_{\text{grid}} = u_{\text{rms}} / (\nu_n k_{\text{Ny}}^{2n-1}) \quad (9)$$

approximately constant. Here, $k_{\text{Ny}} = \pi / \delta x$ is the Nyquist wave number and δx is the mesh spacing. Thus, when doubling the number of meshpoints, we can decrease the viscosity by a factor of about $2^5 = 32$. This shows that hyperviscosity can allow a dramatic increase of the Reynolds number based on the scale of the box. Higher order hyperviscosities

($n=3$ and larger) have been studied previously [12,20], but for us $n=3$ is a practical limit, because we have restricted the maximum stencil length of all derivative schemes to three (in each direction), which is required for sixth order finite difference schemes for our first and second derivatives [21].

In the following we consider the convergence of the energy spectrum for our hyperviscous simulations and compare with direct simulations. We then discuss the Reynolds number dependence of the normalized mean dissipation rate, and finally present the scaling behavior of the structure functions. Our basic conclusion is that in hyperviscous and direct simulations, as well as in wind tunnel experiments, the inertial range scaling is virtually identical and the width of the bottleneck is similar.

A. Energy spectra

Here and below we have calculated the energy dissipation rate from the energy spectrum via

$$\epsilon = 2\nu_n \int k_{\text{eff}}^{2n} E(k) dk. \quad (10)$$

Here we have taken into account that in the code we employ a finite difference scheme which has always a discretization error, so we have to use the effective wavenumber in the expression above. The effective wave number is usually less than the actual one; see Fig. 9.1 of Ref. [21]. For example, for the sixth order finite difference scheme, an analytic expression for k_{eff}^2 was given in Ref. [22], while in the present case we have

$$\kappa_{\text{eff}}^6 = 20 - 30 \cos \kappa + 12 \cos 2\kappa - 2 \cos 3\kappa, \quad (11)$$

where $\kappa = k\delta x$ is the wave number scaled by the mesh spacing δx . Using the effective wave number becomes particularly important in the hyperviscous case in order not to overestimate the contribution to ϵ in Eq. (10).

The dissipation wave number k_d is calculated from the relations $\epsilon = k_d u_{k_d}^3$ and $\epsilon = \nu_n k_d^{2n} u_{k_d}^2$. This leads to

$$k_d^{6n-2} = \epsilon / \nu_n^3 \quad (=k_d^{16} \text{ for } n=3). \quad (12)$$

Again, for $n=1$ one recovers the usual relation $k_d = (\epsilon / \nu^3)^{1/4}$. For larger values of n we find that, in order to make the location of the inertial range in direct and hyperviscous simulations agree, we have to use an effective wave number $k_{d,\text{eff}}$ that is larger than k_d by a factor that is around 4 in our case, i.e., $k_{d,\text{eff}} \approx 4k_d$.

In Fig. 1 we show the convergence of the energy spectra of hyperviscous runs for increasing resolution up to 512^3 meshpoints. All spectra are compensated by a $k^{5/3} \epsilon^{-2/3}$ factor and the abscissa is normalized to the effective dissipation wave number $k_{d,\text{eff}}$. All runs agree in the shape of the bottleneck and the subsequent dissipation subrange, but the length of the inertial range varies from non-existent to about one order of magnitude.

We now compare our 512^3 meshpoints hyperviscous run with the direct simulations of Kaneda *et al.* [4] on the Earth Simulator using 4096^3 meshpoints; see Fig. 2. We see that in both cases the bottleneck sets in at $k/k_{d,\text{eff}} \approx 0.03$ and spans

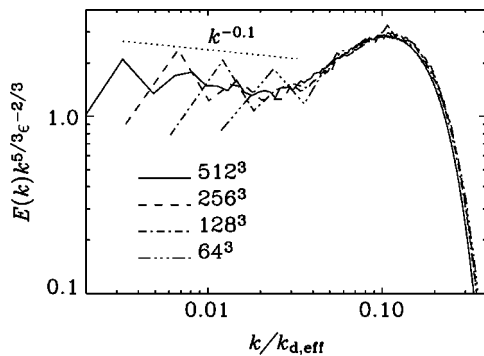


FIG. 1. Time-averaged energy spectra compensated by $k^{-5/3} \epsilon^{-2/3}$. The curves correspond to four different resolutions. All runs are with hyperviscosity.

approximately one decade, but the dissipation subrange is longer in the direct simulations. The height of the bottleneck increases with increasing order of the hyperviscosity [12], which is not surprising given that the steepness of the dissipative subrange is the reason for the bottleneck effect in the first place [1]. In agreement with Kaneda *et al.* [4], we find that the slope of the energy spectrum in the inertial range is consistent with the $k^{-1.77}$ law found in the direct simulation. The Kolmogorov constant is, however, slightly smaller (about $\times 1.1$) in our hyperviscous case.

We should emphasize that, although we solve the compressible equations using finite differences, our direct simulations agree favorably with those using spectral methods solving the incompressible equations. This is shown in Fig. 3 where we compare simulations using 1024^3 meshpoints and normal viscosity with those of Ref. [4]. These data have previously been discussed in Refs. [18,23] in connection with the bottleneck effect in hydrodynamics and hydromagnetic turbulence.

We now compare with the data from a wind tunnel experiment. Ideally we would like to translate the one-

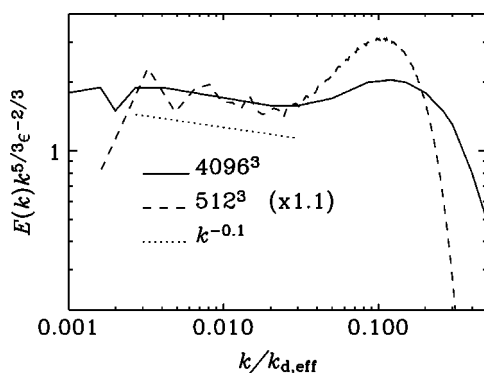


FIG. 2. Time-averaged energy spectra, compensated by $k^{5/3} \epsilon^{-2/3}$, for the direct simulation with 4096^3 meshpoints at $Re_\lambda = 1201$ (solid line) from Fig. 5 of Ref. [4] and our hyperviscous simulation with 512^3 meshpoints (dashed line). Note that the bottleneck has a higher amplitude in the hyperviscous case, but the inertial range has the same slope as for the simulation with 4096^3 meshpoints. Our hyperviscous energy spectrum is scaled by a factor 1.1 in order to make it fall on top of the 4096^3 result, i.e., our Kolmogorov constant is 1.1 times smaller than for the 4096^3 simulation.

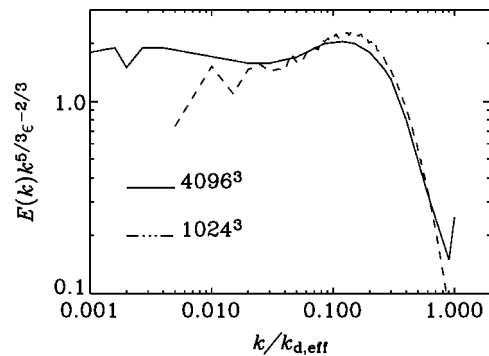


FIG. 3. Our simulation with 1024^3 meshpoints and normal viscosity show a bottleneck very similar to the bottlenecks in Ref. [4], but due to a lack of resolution we do not see any inertial range.

dimensional wind tunnel data into three-dimensional data [18], but this involves differentiation which amplifies the noise in the data. Therefore we now compare one-dimensional energy spectra of our largest hyperviscous simulation with the energy spectrum from a wind tunnel experiment; see Fig. 4. We see that in our simulation the bottleneck has a larger amplitude than in the wind tunnel experiment, but the (negative) slope of the inertial range spectrum is comparable in the two cases, i.e., 1.77. The Kolmogorov constant, on the other hand, is smaller by a factor of 1.5 in the hyperviscous case compared to the wind tunnel experiment.

We feel that the value of a slope of 1.77 should be taken with caution, because it departs rather markedly from the value 1.70 expected from the She-Leveque relation [24]. Given that the inertial range is still relatively short, a slope of 1.70 can certainly not be excluded.

It is customary to quote the Reynolds number based on the Taylor microscale [25]

$$\lambda = \sqrt{5} u_{r.m.s.} / \omega_{r.m.s.} \quad (13)$$

Furthermore, $u_{r.m.s.}$ and $\omega_{r.m.s.}$ are the r.m.s. velocity and vorticity, respectively. One usually takes the one-dimensional r.m.s. velocity for defining the Reynolds number

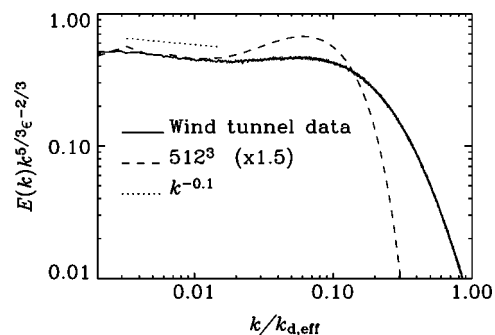


FIG. 4. One-dimensional time-averaged energy spectra of our largest run with hyperviscosity compared with wind tunnel data with $Re_\lambda = 730$ [5]. We have multiplied our energy spectra by 1.5 in order to make it fall on top of the wind tunnel data.

$$\text{Re}_\lambda = u_{1D}\lambda/\nu, \quad (14)$$

where $u_{1D}^2 = \frac{1}{3}u_{r.m.s.}^2$. The wind tunnel experiments have $\text{Re}_\lambda = 730$.

In the hyperviscous case the straightforward definition of the Taylor microscale Reynolds number would be $\text{Re}_\lambda = u_{1D}\lambda^5/\nu_3$, but this would lead to rather large values ($\sim 10^6$) which would not be meaningful in this context. Instead we define an effective viscosity from the actual mean dissipation rate and the modulus of the ordinary rate of strain matrix

$$\nu_{\text{eff}} = \langle \epsilon \rangle / (2\mathbf{S}^2), \quad (15)$$

which is then used to estimate the value of ν in Eq. (14). In this way we find $\text{Re}_\lambda = 340$ for our largest simulation. Comparing with the high resolution direct simulations (Fig. 2) and with wind tunnel data (Fig. 4) we see that $\text{Re}_\lambda = 340$ probably is an underestimate for our hyperviscous simulations.

Alternatively one can define Re_λ as a measure of the width of the inertial range. Using relations that are valid in the standard case with $n=1$, we have $k_{d,\text{eff}}/k_f \sim \text{Re}^{3/4}$ and $\text{Re}_\lambda \sim \text{Re}^{1/2}$, which yields

$$\text{Re}_\lambda \approx \text{Re}_{\lambda 0} \left(\frac{k_{d,\text{eff}}}{k_f} \right)^{2/3}, \quad (16)$$

where we have introduced $\text{Re}_{\lambda 0}$ as a calibration parameter, and k_f is the forcing wave number or, more generally, the wavenumber of the energy carrying scale. If we set $\text{Re}_{\lambda 0} \approx 7.5$, we can reproduce the result $\text{Re}_\lambda = 340$ for our largest run. On the other hand, if we choose to calibrate $\text{Re}_{\lambda 0}$ such that our run with 512^3 meshpoints and the wind tunnel experiments have the same $\text{Re}_\lambda = 730$ (see Fig. 4) then we find $\text{Re}_{\lambda 0} = 16$, which is perhaps a more reasonable estimate.

B. Energy dissipation rate

According to the Kolmogorov phenomenology, the spectral energy flux should be independent of k in the inertial range and equal to both the rate of energy input at large scales and the rate of energy dissipation at small scales. The constant of proportionality is of fundamental interest in turbulence research and one wants to know whether this value is independent of Reynolds number [4,25]. It is customary to define this coefficient as

$$C_\epsilon = \langle \epsilon \rangle L / u_{1D}^3, \quad (17)$$

where $\langle \epsilon \rangle$ is the mean energy dissipation rate and L the integral scale, which is usually defined as $L = (3\pi/4)k_1^{-1}$, where

$$k_1^{-1} = \int k^{-1} E(k) dk \Big/ \int E(k) dk, \quad (18)$$

is the spectrally weighted average of k^{-1} .

The resulting normalized mean energy dissipation rate, calculated in this way, is shown in Fig. 5 as a function of Reynolds number. In the figure diamonds correspond to using Eqs. (14) and (15) to find the Reynolds number, while triangles and plus signs correspond to using Eq. (16) with

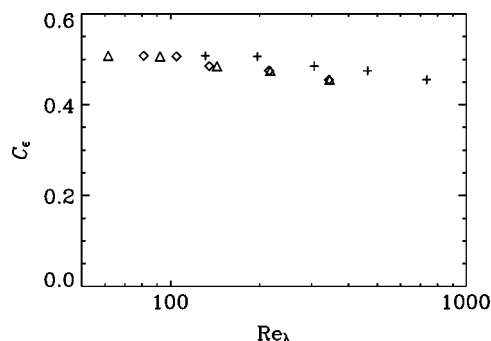


FIG. 5. Plot of C_ϵ as a function of Re_λ for runs with third order hyperviscosity ($n=3$). Triangles and plus signs represent Reynolds numbers calculated based on Eq. (16) with $\text{Re}_{\lambda 0} = 7.5$ and 16, respectively, while for the plus signs Eq. (14) together with Eq. (15) have been used.

$\text{Re}_{\lambda 0} = 7.5$ and 16, respectively. Figure 5 shows that our results are in good agreement with both numerical [4,26] and experimental [25] data.

C. Structure functions

The spectral information can be supplemented by similar scaling information in real space using structure functions. We define the longitudinal and transversal structure functions

$$S_p^{(l)}(r) = \langle \{\hat{r} \cdot [\mathbf{u}(\mathbf{x} + \mathbf{r}) - \mathbf{u}(\mathbf{x})]\}^p \rangle, \quad (19)$$

$$S_p^{(t)}(r) = \langle \{\hat{n} \cdot [\mathbf{u}(\mathbf{x} + \mathbf{r}) - \mathbf{u}(\mathbf{x})]\}^p \rangle, \quad (20)$$

respectively. Here, \hat{r} is the unit vector of \mathbf{r} and \hat{n} is normal to \mathbf{r} , so $\hat{n} \cdot \hat{r} \equiv 0$. The structure function of the three-dimensional velocity field

$$S_p(r) = \langle |\mathbf{u}(\mathbf{x} + \mathbf{r}) - \mathbf{u}(\mathbf{x})|^p \rangle \quad (21)$$

can then be written as

$$S_p(r) = \frac{1}{3} [S_p^{(l)}(r) + 2S_p^{(t)}(r)]. \quad (22)$$

We define the p th order structure function scaling exponent, ζ_p via the scaling relation

$$S_p(r) \propto r^{\zeta_p}. \quad (23)$$

In Fig. 6 we plot the derivative of the double-logarithmic slope of the structure functions $d \ln S_p / d \ln r$. Inertial range scaling is indicated by a plateau in this graph. We find from the lower curve of Fig. 6 that $\zeta_2 \approx 0.7$. More importantly, in the upper curve of Fig. 6, we show that $S_3(r)$ is consistent with linear scaling, i.e., $\zeta_3 = 1$. Knowing this we can use the extended self-similarity [27] to find the other structure function scaling exponents. The results are shown in Fig. 7 where we see that the longitudinal structure function exponents follow the She and Leveque [24] scaling very well, while the transversal structure function is slightly more intermittent (i.e., the graph of ζ_p versus p is more strongly bent). In particular we note that the extended self similarity gives $\zeta_2 = 0.696$ for the longitudinal component.

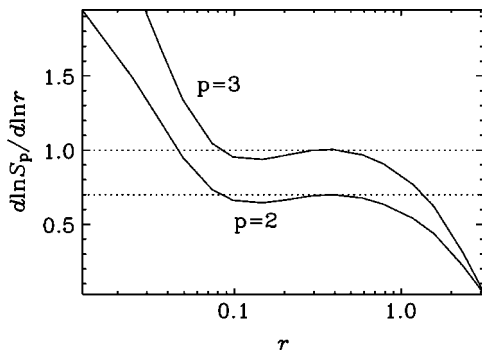


FIG. 6. Time-averaged total structure functions $[S_p^{(l)} + 2S_p^{(o)}]/3$ for $p=2$ and $p=3$. The two dotted horizontal lines go through 0.7 and 1.0, confirming the expected scaling from the She-Leveque relationship.

D. Decaying turbulence

Decaying isotropic turbulence is often considered an important benchmark of turbulence theories, and comparisons with wind tunnel experiments and large eddy simulations are available [28]. We have carried out simulations of decaying turbulence by stopping the driving at a time that will now be redefined to $t=0$. In Fig. 8 we show that asymptotically

$$\langle u^2 \rangle / u_0^2 = (t/\tau)^n, \quad (24)$$

where u_0 is the initial ($t=0$) r.m.s. velocity and τ is a constant obtained from the intersection of the decay law extrapolated to $\langle u^2 \rangle = u_0^2$. It turns out that our law is consistent with $n = 1.25$, which is in agreement with recent wind tunnel data and large eddy simulations [28].

The bottleneck effect is roughly unchanged; see Fig. 9. Its width is still about one order of magnitude in wave number, which is comparable to the experimental results [28]. The height of the bottleneck is much less in the experimental data, because they show only a one-dimensional spectrum which gives a much weaker hump than the three-dimensional spectra [18]. In any case, we know already that the height of the bottleneck is artificially enhanced by the use of hyperviscosity.

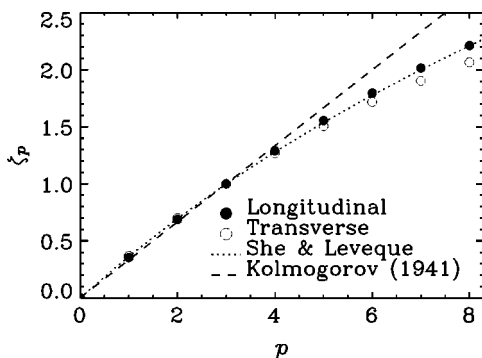


FIG. 7. Structure function scaling exponents found using the concept of extended self similarity. We see that the longitudinal scaling exponents follow the She and Leveque scaling very well, while the transversal scaling exponents are somewhat more intermittent.

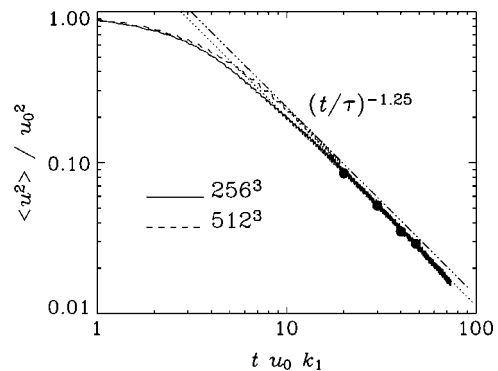


FIG. 8. Mean squared velocity as a function of time for a simulation where the forcing has been stopped at $t=t_0$. In the 256^3 simulation we have $Re_{\text{grid}}=0.20$ (based on the initial value u_0) and $\tau u_0 k_1=2.8$ while in the 512^3 simulation we have $Re_{\text{grid}}=0.24$ and $\tau u_0 k_1=3.1$. The solid circles correspond to the experimental results of Kang *et al.* [28].

In the present decay simulations one also sees the beginning of a subinertial range, leaving only a very short inertial range around $0.1 \leq k(\nu_3 t)^{1/6} \leq 0.3$. The slope is compatible with the She-Leveque slope of 1.70, which corresponds to a residual slope of $k^{-0.03}$ after compensating with $k^{5/3}$. Thus, there is no longer evidence for the more extreme correction of -0.1 suggested by the forced turbulence simulations [4].

IV. CONCLUSION

The present investigations have shown that turbulence simulations with hyperviscosity are able to reproduce virtually the same inertial range scalings as simulations with ordinary viscosity. Specifically, the structure function exponents show scaling behavior that is consistent with the She-Leveque [24] model. However, the transversal structure functions show a slightly higher degree of intermittency than

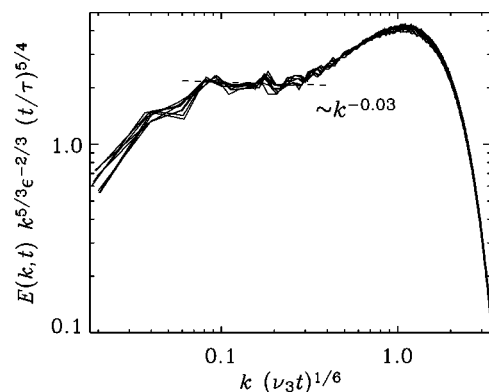


FIG. 9. Energy spectra for a decaying run. The abscissa is compensated by $(\nu_3 t)^{1/6}$ to make it dimensionless and to account for the slow decrease of the dissipation wavenumber. The ordinate is compensated by $k^{5/3} \epsilon^{-2/3}$ to show the location of the inertial range and by $t^{5/4}$ to compensate for the decay.

the longitudinal ones. This, in turn, is quite consistent with a number of turbulence simulations by other groups [29,30]. A possible explanation for the difference between longitudinal and transversal structure functions has been offered by Siefert and Peinke [31], who find different cascade times for longitudinal and transversal spectra. The spectra show inertial range scaling similar to that found both in wind tunnel experiments [5] and in very high resolution direct simulations [4]. In all three cases (hyperviscous and direct simulations as well as wind tunnel experiments) the inertial range spectrum is found to be compatible with the $k^{-1.77}$ behavior found by Kaneda *et al.* [4]. As discussed above, this result is not compatible with the results from the structure function scalings and the She-Leveque relation. However, we believe that the presently resolved inertial range is still too short to distinguish conclusively between 1.77 and the She-Leveque value of 1.70. Also, the simulation data of decaying turbulence suggest a weaker correction of 0.03, giving a slope of 1.70 that is compatible with the She-Leveque scaling.

Another important result is that the width of the bottleneck seems to be independent of the use of hyperviscosity, and that only its height increases with the order of the hyperviscosity. This result is also confirmed in the case of decaying turbulence. Finally, we note that the normalized dissipation rate is independent of the Reynolds number, and that the asymptotic value of $C_\epsilon \approx 0.5$ is in agreement with both experimental and numerical results [4,32].

One should of course always be concerned about the possible side effects of using hyperviscosity. One worry is that hyperviscosity may actually affect almost all of the inertial subrange [13,14]. The current simulations confirm that the

bottleneck requires at least an order of magnitude in k space, and so does the dissipative subrange, leaving almost no inertial range at all—even in a simulation with 1024^3 mesh points. Thus, using hyperviscosity appears to be a reasonable procedure for gaining information about the inertial range at moderate cost, even though one should still use a reasonably high resolution to isolate true inertial range features from those in the bottleneck subrange. On the other hand, hyperviscosity is not a universally valid approximation. An example is in magnetohydrodynamics when magnetic helicity is finite and a large scale magnetic field builds up in a closed or fully periodic box [33]. As long as it is possible to understand the origin of peculiar features arising from hyperviscosity or hyper-resistivity (as is the case in helical hydro-magnetic turbulence) there may well be circumstances where turbulence with hyperviscosity can provide a useful model for certain studies. One should bear in mind, however, that the height of the bottleneck depends on the order of the hyperviscosity. For example, if we choose $n > 3$ in Eq. (2), the height of the bottleneck will be even more exaggerated [12].

ACKNOWLEDGMENTS

We acknowledge the very valuable help and discussions with B. R. Pearson. We thank the Danish Center for Scientific Computing for granting time on the Horseshoe cluster, and the Norwegian High Performance Computing Consortium (NOTUR) for granting time on the parallel computers in Trondheim (Gridur/Embla) and Bergen (Fire).

-
- [1] G. Falkovich, *Phys. Fluids* **6**, 1411 (1994).
 - [2] D. Lohse and A. Müller-Groeling, *Phys. Rev. Lett.* **74**, 1747 (1995); *Phys. Rev. E* **54**, 395 (1996).
 - [3] Z.-S. She and E. Jackson, *Phys. Fluids A* **5**, 1526 (1993).
 - [4] Y. Kaneda, T. Ishihara, M. Yokokawa, K. Itakura, and A. Uno, *Phys. Fluids* **15**, L21 (2003).
 - [5] B. R. Pearson, P. Å. Krogstad, and G. R. Johnson, in *Reynolds Number Scaling in Turbulent Flow*, edited by A. J. Smith (Kluwer Academic, Dordrecht, 2003), pp. 229-236.
 - [6] D. H. Porter, P. R. Woodward, and A. Pouquet, *Phys. Fluids* **10**, 237 (1998).
 - [7] T. Gotoh and D. Fukayama, *Phys. Rev. Lett.* **86**, 3775 (2001).
 - [8] C. Basdevant, B. Legras, R. Sadourny, and M. Beland, *J. Atmos. Sci.* **38**, 2305 (1981).
 - [9] M. Meneguzzi, U. Frisch, and A. Pouquet, *Phys. Rev. Lett.* **47**, 1060 (1981).
 - [10] J. C. McWilliams, *J. Fluid Mech.* **146**, 21 (1984).
 - [11] T. Passot and A. Pouquet, *J. Comput. Phys.* **75**, 300 (1988).
 - [12] V. Borue and S. Orszag, *Europhys. Lett.* **29**, 687 (1995).
 - [13] D. Biskamp, E. Schwarz, and A. Celani, *Phys. Rev. Lett.* **81**, 4855 (1998).
 - [14] D. Biskamp and W.-C. Müller, *Phys. Plasmas* **7**, 4889 (2000).
 - [15] G. K. Batchelor, *The Theory of Homogeneous Turbulence* (Cambridge University Press, Cambridge, 1953), p. 50.
 - [16] J. O. Hinze, *Turbulence*, 2nd ed. (McGraw-Hill, New York, 1975), p. 202.
 - [17] A. S. Monin and A. M. Yaglom, *Statistical Fluid Mechanics* (MIT Press, Cambridge, MA, 1987), Vol. 2, Sec. 12.
 - [18] W. Dobler, N. E. L. Haugen, T. A. Yousef, and A. Brandenburg, *Phys. Rev. E* **68**, 026304 (2003).
 - [19] <http://www.nordita.dk/software/pencil-code/>
 - [20] J. Cho, A. Lazarian, and E. Vishniac, *Astrophys. J.* **595**, 812 (2003).
 - [21] A. Brandenburg, in *Advances in Nonlinear Dynamics. The Fluid Mechanics of Astrophysics and Geophysics*, edited by A. Ferriz-Mas and M. Núñez (Taylor & Francis, London, 2003), Vol. 9, p. 269.
 - [22] M. Christensson, M. Hindmarsh, and A. Brandenburg, *Phys. Rev. E* **64**, 056405 (2001).
 - [23] N. E. L. Haugen, W. Dobler, and A. Brandenburg, *Phys. Rev. E* **70**, 016308 (2004).
 - [24] Z.-S. She and E. Leveque, *Phys. Rev. Lett.* **72**, 336 (1994).
 - [25] K. R. Sreenivasan, *Phys. Fluids* **10**, 528 (1998).
 - [26] B. R. Pearson, T. A. Yousef, N. E. L. Haugen, A. Brandenburg, and P. Å. Krogstad, e-print physics/0404114.
 - [27] R. Benzi, S. Ciliberto, R. Tripicciono, C. Baudet, F. Massaioli,

- and S. Succi, Phys. Rev. E **48**, R29 (1993).
- [28] H. S. Kang, S. Chester, and C. Meneveau, J. Fluid Mech. **480**, 129 (2003).
- [29] T. Gotoh, Comput. Phys. Commun. **147**, 530 (2002).
- [30] D. Porter, A. Pouquet, and P. Woodward, Phys. Rev. E **67**, 026301 (2002).
- [31] M. Siefert and J. Peinke, e-print physics/0309106.
- [32] B. R. Pearson, P. Å. Krogstad, and W. van de Water, Phys. Fluids **14**, 1288 (2002).
- [33] A. Brandenburg and G. R. Sarson, Phys. Rev. Lett. **88**, 055003 (2002).